# Control Optimization of Modular Multilevel Resonant DC Converters for Wide-Input-Range MVdc to LVdc Applications

Jing Sheng, *Graduate Student Member, IEEE*, Cong Chen, Rui Lu, *Graduate Student Member, IEEE*, Chushan Li, *Member, IEEE*, Xin Xiang, *Member, IEEE*, Wuhua Li, *Member, IEEE*, and Xiangning He, *Fellow, IEEE*

***Abstract*—In this article, the output voltage control strategy of modular multilevel resonant dc converters (MMRDC) for medium-voltage wide-input-range applications is studied. First, the feasibility and influence of the switching frequency regulation and modulation index regulation are investigated in detail. It is found that the switching frequency choice has a significant effect on the voltage stress of arm inductors and the transformer. Then, based on these considerations, the modulation index regulation plus switching frequency regulation based design and control optimization is proposed. With the proposed design and control method, the switching frequency range for adapting to a wide input range is further reduced, especially under light load operating conditions. Besides, the high voltage stress on arm inductors is avoided and the high voltage *dv/dt* on the transformer is also eliminated. Finally, a laboratory prototype with 8–16 kV input and 375 V/60 kW output has been built and the experimental validation under a wide input range has been done. The efficiency over 96.4% under the wide input range proved the effectiveness of the optimized control methods.**

***Index Terms*—Medium-voltage dc (MVdc), modulation index regulation, modular multilevel resonant dc converter (MMRDC), switching frequency regulation, wide input range.**

## I. Introduction

With the rapid development of renewable energy power generation, electrical rail transportation, and data centers in recent years, the medium-voltage dc (MVdc) power distribution systems have attracted much research interest in the academic and industrial world owing to their high efficiency, high power quality, and high stability [1]–[4]. In these MVdc applications, dc–dc converters, also called dc transformers, are the key roles to connect different voltage level dc grids or convert MVdc voltage to low-voltage dc (LVdc) voltage for power supply [5]–[7].

In the low-voltage dc–dc conversion, many topologies and control methods have been researched for many years, such as half-bridge, full-bridge, resonant converters, and other series of isolated or nonisolated structures [8]. Usually, a single power switch device can fulfill the voltage and current requirements for low-voltage converters. However, in MV applications, devices, modules, or converters connected in series and parallel are an essential way [9], [10], even though some dc transformers based on high-voltage devices are developed [4], [11]. Typically, a solution for MVdc to LVdc conversion is the input-series output-parallel (ISOP) structure, which has been intensively studied and widely used due to its modularity and easy control. However, there are many high-frequency (HF) transformers in an isolated ISOP converter. Thus, under a medium voltage over 10 kV, the primary and secondary sides of the HF transformer will withstand the insulation of tens of kilovolts. Consequently, the volume of the modules will be significant and the power density could be small [12], [13]. These drawbacks limit the promotion of an ISOP structure in higher voltage and higher power applications.

One feasible solution for these problems is the modular multilevel topology with a centralized transformer. The modular multilevel structure using submodules (SMs) in series has good modularity and flexibility, suitable for extending input voltage and power rating [14], [15]. A centralized high-power transformer features easier insulation isolation, higher power density, and easier manufacturing than multiple distributed low power transformers [13], [16]. In recent years, a lot of literature proposed modular multilevel converter (MMC) based dc–dc topologies for MVdc conversion, such as dual-active-bridge (DAB) structure and resonant structure [16]–[20]. In the MVdc application, the high switching frequency (tens of kilohertz) is preferred owing to low-voltage switching devices' good features rather than a medium frequency of hundreds of hertz in the HVdc application. So, the transformer volume and other passive

Manuscript received July 14, 2021; revised October 19, 2021; accepted November 27, 2021. Date of publication December 9, 2021; date of current version January 19, 2022. This work was supported in part by the National Nature Science Foundations of China under Grants 51807176 and 52107214 and in part by the National Nature Science Foundation of China for China-U.K. Joint Project under Grant 52061635101. Recommended for publication by Associate Editor D. O. Neacsu. *(Corresponding authors: Chushan Li; Xin Xiang.)*

Jing Sheng, Cong Chen, Rui Lu, Xin Xiang, Wuhua Li, and Xiangning He are with the College of Electrical Engineering, Zhejiang University, Hangzhou 310027, China (e-mail: zjdxsj2013@zju.edu.cn; 22010153@zju.edu.cn; lurui@zju.edu.cn; xiangxin@zju.edu.cn; woohualee@zju.edu.cn; hxn@zju.edu.cn).

Chushan Li is with the Zhejiang University–University of Illinois at Urbana-Champaign Institute, Zhejiang University, Haining 314400, China, and also with the College of Electrical Engineering, Zhejiang University, Hangzhou 310027, China (e-mail: lichushan@hotmail.com).

Color versions of one or more figures in this article are available at https://doi.org/10.1109/TPEL.2021.3133174.

Digital Object Identifier 10.1109/TPEL.2021.3133174

devices will be reduced remarkably [21]–[23]. Moreover, MMC SM switches can achieve zero-voltage-switching (ZVS) on operation [24]. As a result, the switching losses decrease under high switching frequency operation.

In some MVdc to LVdc power supply applications, the input medium voltage may vary over a wide range [25]–[28]. For example, in a large-scale submarine observatory network system, a 15 kV voltage source onshore power the scientific observation instruments thousands of kilometers away through a single submarine cable. Because the subsea cable is limited by its insulation and manufacturing cost, the cable resistance is much larger than the overhead line on land. Generally, the parasitic resistance is about 1 Ω per 1 km for a 15-kV submarine cable. There will be a 5 kV voltage drop on a 500-km cable when the input current ranges from 0 to 10 A. Thus, an MVdc to LVdc converter with a wide voltage-gain range is necessary to power the large-scale submarine instruments. The cable can be laid further away from onshore based on this kind of wide voltage-gain range MVdc converters. More large power instruments can be installed and work simultaneously, which is valuable for long-term, uninterrupted ocean observation [29]–[31].

Several degrees of freedom (DOF), such as switching frequency, phase shift angle, and SM duty cycle, have been used to change the voltage gain of MMC-based dc–dc converters. By now, most of the existing literature tends to regulate the phase shift angle in various ways. For example, most MMC dc–dc converters are usually modulated to a quasi-square wave (QSW). Each SM has a slight phase shift angle. QSW modulation can enhance the dc voltage utilization, mitigate the *dv*/*dt* stress on the HF transformer, diminish the common-mode component of arm current, and achieve soft switching of SM devices [32]. In [33], trapezoidal modulation has been discussed to change the fundamental voltage amplitude of MMC unit output (increase the phase shift angle among arm SMs). This method can achieve a narrow modulation index ranging from 0.81 to 1.27. According to the comprehensive analysis of [34], the SM switches will lose the soft switching, having the highest current stress and lowest efficiency under triangular modulation compared with that under square modulation. Besides, some advanced modulation strategies regulate the phase shift angle between the phase legs or between the primary and secondary sides, such as single phase shift and dual phase shift [35], [36]. However, the phase shift control will increase the reactive power inside MMC [25], [37].

In [16] and [17], the modular multilevel resonant dc converter (MMRDC) with MMC and *LLC*'s inherited advantages was first proposed. Furthermore, regulating the number of inserted SMs rather than a fixed number of inserted SMs is employed to adapt wide-range input in [16]. Fortunately, the *LLC* resonant unit can work within a much narrower switching frequency. However, the criteria of selecting the inserted SM number and the switching frequency range are not well designed, which will result in a very high switching frequency under light load [38], [39]. Besides, the influence of switching frequency on MMRDC has not been investigated in-depth in the existing papers.

This article proposes an optimized control strategy to solve the problems mentioned above. The contributions can be summarized as three aspects. First, based on the analysis of MMRDC working modes under different switching frequencies, this article finds that the input medium voltage will be applied to the arm inductors when the switching frequency is larger than the *LLC* main resonant frequency. Moreover, a very high *dv*/*dt* will be applied on the primary side of the HF transformer, threatening the insulation safety. Second, a novel criterion of modulation index control is proposed to calculate how many SMs should be inserted with different input voltages. The optimized switching frequency under any load conditions is restricted to a narrow range. In addition, the optimization control avoids the high voltage stress on arm inductors and the transformer. Third, the optimized control strategy requires a larger magnetizing inductance of the transformer than the existing control. Larger magnetizing inductance produces a smaller magnetizing current, reducing the conduction losses of SMs devices and transformer windings. More critically, larger magnetizing inductance reduces the transformer core's air gap and accordingly reduces the core loss. Thus, it is much easier for transformer design and manufacture.

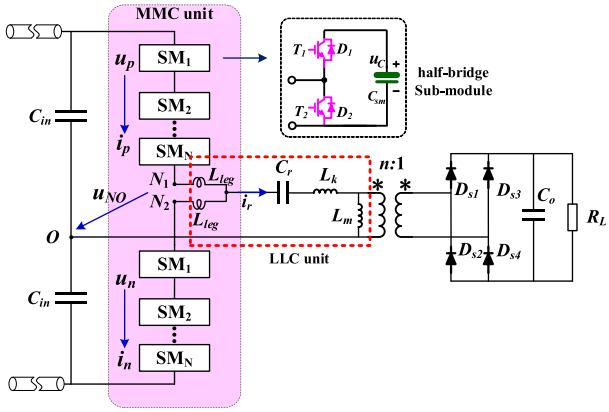


Fig. 1. MMRDC topology.

The rest of this article is organized as follows. Based on the operation principles of MMRDC in Section II, the two control DOF of MMRDC are studied. Section III deeply investigates the modulation index regulation plus switching frequency regulation based voltage control strategy for wide-input-range MMRDC. In Section IV, a laboratory 16-kV/60-kW prototype has been built and the experiment results are presented. The medium-voltage converter can operate with the same high efficiency of 96.4% under 8–16k V input range, by employing the optimized voltage control strategy. Finally, Section V concludes this article.

## II. Fundamentals of MMRDC

### A. Basic Operation Principles

Half-bridge *LLC* resonant converters are widely used in low-voltage dc applications owing to their high efficiency and high power density. Suppose series-connected SMs replace the two switches in a half-bridge *LLC* resonant converter to withstand the input high voltage. In that case, the modular multilevel resonant converter (MMRC) is obtained, as shown in Fig. 1. In Fig. 1, the input capacitor $C_{\rm in}$ provides the midpoint of input voltage

TABLE I
SM DEVICES SOFT-SWITCHING STATES

| Working conditions | T1 | D1 | T2 | $D_2$ |
|---|---|---|---|---|
| $i_{dc} < i_m/2$ | ZVS ON hard OFF | ZCS OFF | ZVS ON hard OFF | ZCS OFF |
| $i_{dc} > i_m/2$ | ZVS ON ZCS OFF | hard OFF | hard ON hard OFF | no switching |

for the *LLC* unit and absorbs the ac component of the MMC arm current. The arm inductors in the MMC unit are reserved for three purposes. One is for mitigating the current impact when arm SM capacitors are switched in and out. Another is for mitigating the arm circulating current, although the circulating current component is small under QSW modulation [20]. The third one is as a part of the resonant inductance because the *LLC* resonant inductance is composed of MMC arm inductors and isolation transformer leakage inductance expressed as follows:

$$L_r = {}^1\!/_2 L_{leg} + L_k. \tag{1}$$

The MMC unit generates a quasi-square waveform on the *LLC* unit, and the *LLC* unit operates the same as the traditional *LLC* circuit. The resonant current $i_r$ consists of magnetizing current $i_m$ and fundamental active current. $i_r$ is divided equally by MMC upper arm and lower arm. Considering that the MMC circulating current is very small, the arm voltage $u_p/u_n$ and arm current $i_p/i_n$ can be expressed as the following equations [40]:

$$\begin{cases} u_p = {}^1\!/_2 u_{dc} - u_{ac} \\ u_n = {}^1\!/_2 u_{dc} + u_{ac} \end{cases} \tag{2}$$

$$\begin{cases} i_p = i_{dc} + {}^1\!/_2 i_r \\ i_n = i_{dc} - {}^1\!/_2 i_r \end{cases} \tag{3}$$

where $u_{dc}$ is the input dc voltage, $u_{ac}$ is the MMC output ac voltage, and $i_{dc}$ is the input dc current.

The typical operation waveforms under different load conditions are shown in Fig. 2. QSW modulation is usually adopted to improve the dc voltage utilization and alleviate the high *dv*/*dt*. The SMs are inserted and bypassed with a very small delay.

Different from the half-bridge *LLC* converter, the soft-switching of SMs is not determined by the switching frequency or *LLC* resonant mode but decided by the arm current direction of the switching point. From the current direction illustrated in Fig. 2(a) and (b), the two switches ($T_1$ and $T_2$) of half-bridge SM can achieve ZVS ON but hard-switching OFF if the dc current $i_{dc}$ is smaller than the magnetizing current $i_m/2$. The antiparallel diodes $D_1$ and $D_2$ have zero-current switching (ZCS) OFF. However, under heavy load conditions, if the dc current $i_{dc}$ is larger than the magnetizing current $i_m/2$, $T_2$ and $D_1$ lose the soft switching ability and $T_1$ has ZVS ON and ZCS OFF. The soft switching features of SM devices are given in Table I. Moreover, according to Fig. 2(c), the four diodes $D_{s1}$–$D_{s4}$ in the low voltage side can always be soft switched OFF due to the resonant current turning to zero naturally.

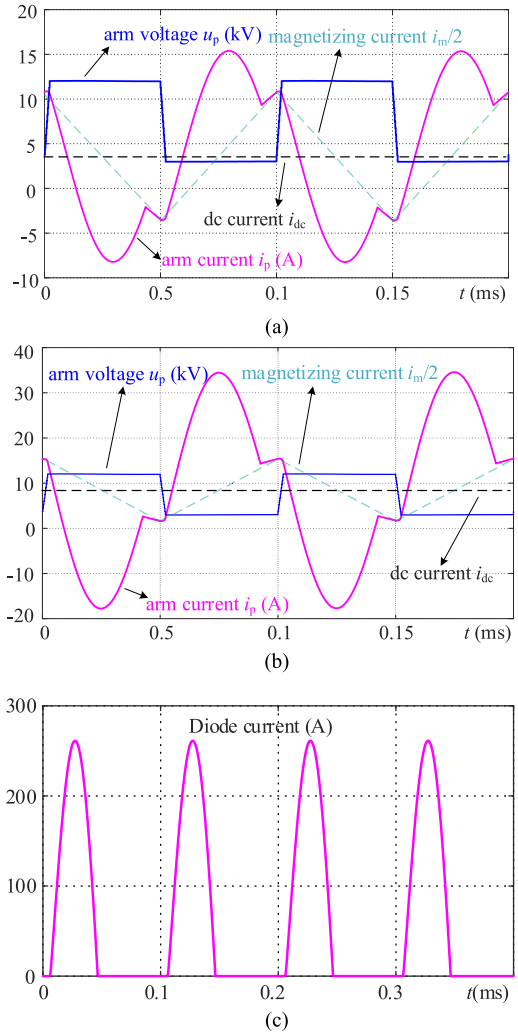


Fig. 2. Operation waveforms of MMRDC. (a) Arm voltage and arm current under light load conditions, i.e., when $i_{dc} < i_m/2$. (b) Arm voltage and arm current under heavy load conditions, i.e., when $i_{dc} > i_m/2$. (c) LV side diode current.

## B. Modulation Method

The QSW modulation can obtain a high dc voltage utilization and low *dv*/*dt* on the transformer. Usually, a simple approach to generate the quasi-square waveform in the actual implementation, called phase shift modulation, is indicated in Fig. 3(a). Two kinds of inserted status of half-bridge SMs are presented in Fig. 3(b). One is called "half-inserted," which means the SM inserted duty cycle is 50% in one switching period. Another state is called "full-inserted," meaning the SM is always inserted in one switching period. A tiny phase shift angle $\varphi$ is set among the half-inserted SMs to reduce the sharp *dv*/*dt*. For example, suppose that there are *K* full-inserted SMs and *N*-*K* half-inserted SMs in one period. In that case, the arm voltage of MMRDC is a quasi-square waveform from $KU_C$ to $NU_C$, where *N* is the arm SM number and $U_C$ represents the SM capacitor voltage.

Due to the phase shift angle among these SMs, the capacitor voltage balancing control is easy to implement and some effective balancing strategies of MMC-based dc–dc converters

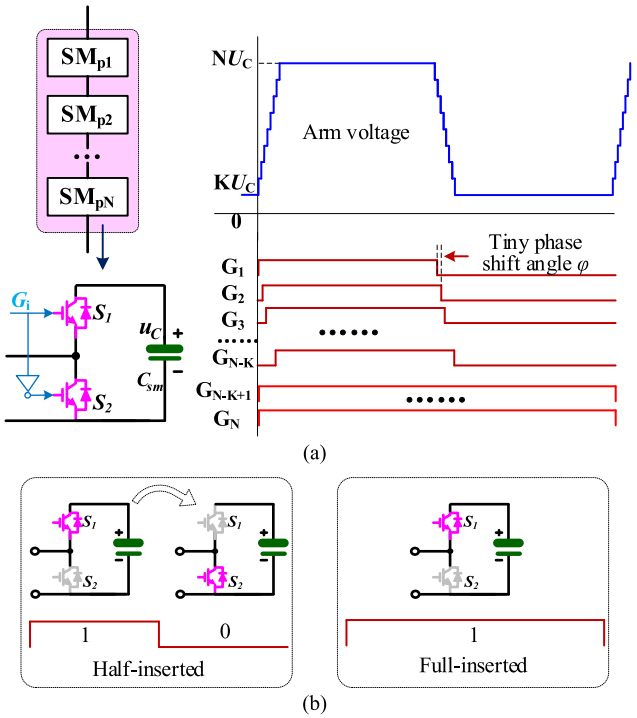


Fig. 3. Typical QSW modulation method with a slight phase shift angle. (a) Phase shift modulation for MMRC. (b) Two kinds of SM inserted status in one switching period.

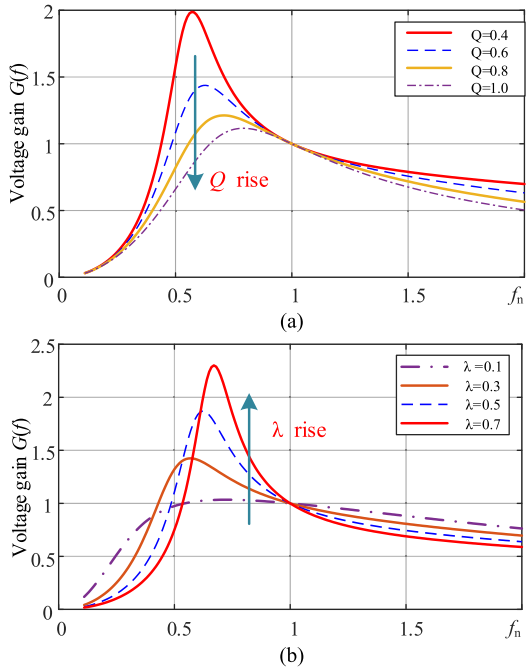


Fig. 4. *LLC* unit gain under different switching frequency. (a) *LLC* gain with different quality factors $Q$. (b) *LLC* gain with different inductor ratios λ.

with phase shift modulation have been proposed in [16], [41], and [42]. The SM voltage balancing algorithm in [16] is used in this article. The controller sorts these arm capacitor voltage variations during the last period and reassigns the gate signals according to their different charge abilities. For example, distribute the gate signal with the biggest charge ability to the SM with the lowest voltage vice versa.

## III. Proposed Output Voltage Control Optimization

### A. Traditional Frequency Regulation Control

MMRDC converters inherit the good control flexibility of MMC topology and high efficiency of *LLC* resonant topology. The *LLC* unit can change the switching frequency to regulate the gain of the *LLC* unit. The approximate gain expression and gain curve of the *LLC* unit is written in the following equation and drawn in Fig. 4:

$$G(Q,\lambda,f_{\rm n})=\frac{1}{\sqrt{\left(1+\lambda-\frac{\lambda}{f_{\rm n}^2}\right)^2+Q^2\left(f_{\rm n}-\frac{1}{f_{\rm n}}\right)^2}} \tag{4}$$

$$f_{\rm r}=\frac{1}{2\pi\sqrt{C_{\rm r}L_{\rm r}}},\ f_{\rm n}=f_{\rm s}/f_{\rm r} \tag{5}$$

where $f_{\rm n}$ is the normalized switching frequency, $Q$ is the quality factor, and λ is the inductor ratio defined as follows:

$$Q=\frac{\sqrt{L_{\rm r}/C_{\rm r}}}{R_{\rm eq}} \tag{6}$$

$$\lambda=L_{\rm r}/L_{\rm m}. \tag{7}$$

where $R_{\rm eq}$ is the equivalent resistance in the transformer primary side.

According to Fig. 4, when $Q$ rises (which means the output power rises), the *LLC* gain range decreases markedly, and when λ decreases (which means the magnetizing inductance rises), the *LLC* gain range decreases [43]. Consequently, the switching frequency range will be very large if the input voltage and output power vary in a wide range. Then, the *LLC* parameters design will be troublesome and the conversion efficiency will be low under a wide switching frequency range, especially in medium-voltage applications.

### B. Influence of Switching Frequency for MMRDC

It is well-known that in the low-voltage *LLC* converters, the switching frequency can be designed larger than the resonant frequency to increase the voltage gain range and achieve the soft switching of power devices. However, in medium-voltage MMRDC converters, the influence of switching frequency is much different from that in LV *LLC* converters. First, the soft switching state of MMC SM devices is decided by arm direction at the switching time rather than the switching frequency. So the design of soft switching can be decoupled from switching frequency. Second, under light load conditions ($Q=0.4$), as shown in Fig. 4(a), the *LLC* unit gain changes much more gently with switching frequency when $f_{\rm n}>1$. Therefore, it is not an economical and efficient way to obtain a larger gain range by improving the switching frequency in MV applications.

Third, if the switching frequency is larger than the *LLC* resonant frequency, the *LLC* unit will turn into *LC* resonant mode. In this operation mode, the resonant current $i_{\rm r}$ is continuous, which means that the currents through inductors and

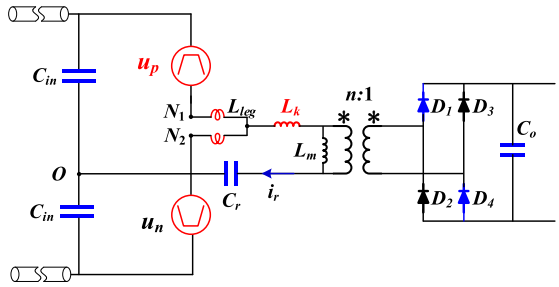


Fig. 5. Equivalent circuit of MMRDC.

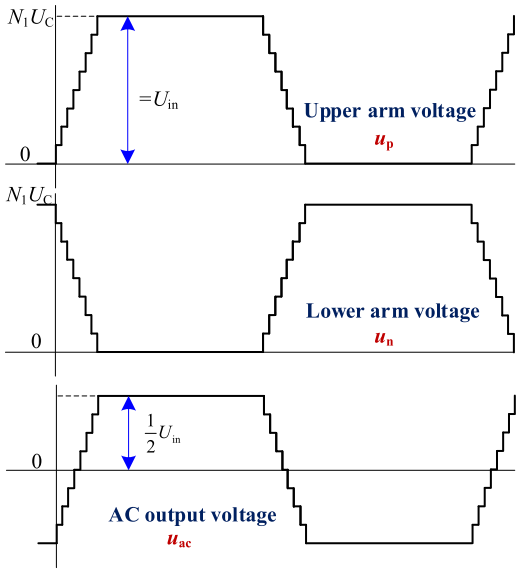


Fig. 6. Traditional QSW modulation for MMC-based dc–dc converters.

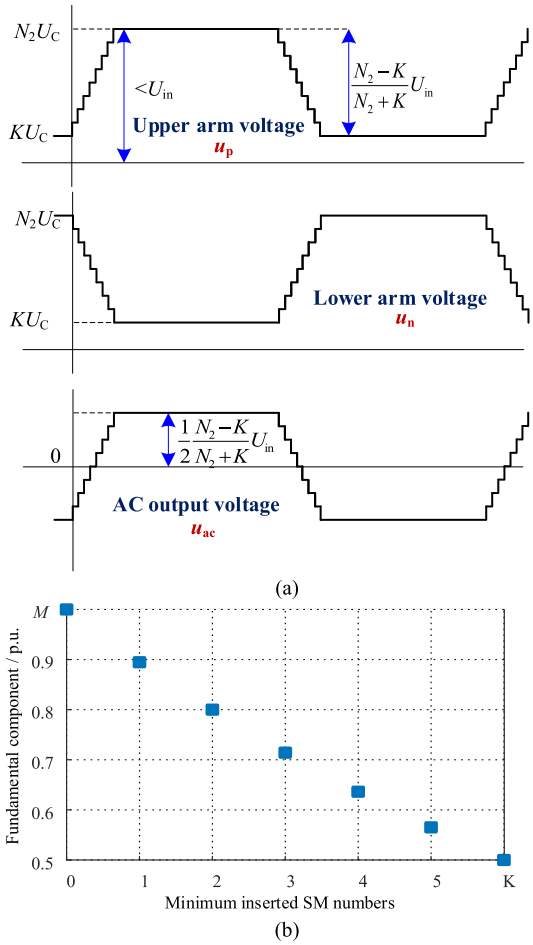


Fig. 7. Modulation index control of MMRDC. (a) Variable modulation index with different inserted SM numbers. (b) Relationship between the modulation index and minimum inserted SMs.

secondary side diodes are always continuous. Referring to the simplified equivalent circuit of the MMRDC converter in Fig. 5, the secondary-side voltage of the HF transformer is clamped by the output dc voltage. Therefore, the voltage on the transformer windings is a complete square shape and a very high *dv/dt* will be imposed on the primary windings. Moreover, according to Kirchhoff's voltage law, the quasi-square waveform generated by MMC arm SMs will be directly imposed on the MMC arm inductors simultaneously. As a result, a very high voltage spike would emerge on MMC arm inductors. In MV applications, these issues will cause serious insulation challenges to the transformer and inductor design.

### C. Modulation Index Regulation Control

Fig. 6 presents the traditional modulation without modulation index control for MMC based dc–dc converters. The upper arm and lower arm waveforms are complementary. The minimum and maximum values of arm voltage are 0 and the input dc voltage $U_{\rm in}$, respectively. Therefore, the number of arm SMs $N_1$ is determined by maximum input dc voltage $U_{\rm dc,max}$ and rated SM capacitor voltage $U_{\rm C}$, indicated as follows:

$$N_1 = U_{\rm dc,max}/U_C. \tag{8}$$

Fortunately, one advantage of the MMC converters is that the shape of the MMC output voltage can be easily regulated. Hence, the voltage gain of MMC can be controlled by changing the shape of the MMC output waveform. A possible way is to change the waveform amplitude by inserting a different number of SMs [44].

In this article, adjusting the minimum inserted SM numbers in one switching period is employed to change the MMC modulation index. Specifically, if the input voltage is the minimum, the minimum inserted SM number is 0. When the input voltage increases, the minimum inserted SM number will be set to $K$ ($K = 0, 1, 2, 3, \ldots,$). In this case, the modulation method is illustrated in Fig. 7(a). In one switching period, $K$ SMs are full-inserted states and $N_2$-$K$ SMs are half-inserted states, where $N_2$ is the MMC arm SM number. The MMC upper and lower arm voltages are still complementary. Unlike Fig. 6, the arm voltage steps from $KU_{\rm C}$ to $N_2U_{\rm C}$ in Fig. 7(a).

Based on the waveforms in Fig. 7(a) and arm voltage (2), the input voltage and ac output voltage can be expressed as follows:

$$\begin{cases} U_{\rm dc} = |u_{\rm p} + u_{\rm n}| = N_2U_C + KU_C \\ U_{\rm ac} = |1/2\,(u_{\rm n} - u_{\rm p})| = 1/2\,(N_2U_C - KU_C) \end{cases} \tag{9}$$

where $U_{\rm dc}$ is the input dc voltage, $u_{\rm p}/u_{\rm n}$ are the arm voltages, and $U_{\rm ac}$ is the amplitude of the MMC ac output voltage.

From (9), the capacitor voltage $U_{\rm C}$ can be calculated through dc voltage $U_{\rm dc}$, SM numbers $N_2$, and $K$ as

$$U_C = \frac{U_{\rm dc}}{N_2 + K}. \tag{10}$$

Substituting (10) into (9) yields

$$U_{\rm ac} = \frac{N_2 - K}{N_2 + K} \cdot \frac{1}{2} U_{\rm dc} = M(K) \cdot \frac{1}{2} U_{\rm dc} \tag{11}$$

where $M(K)$ stands for the modulation index of the MMC unit defined by

$$M(K) = \frac{N_2 - K}{N_2 + K}. \tag{12}$$

From (9) and (10), the dc input voltage is supported by $N_2+K$ SMs. So, the arm SM number $N_2 = U_{\rm dc}/U_{\rm C} - K$ is smaller than the traditional design value $N_1 = U_{\rm dc}/U_{\rm C}$, which is a benefit of the modulation index control.

Given arm SM number $N = 18$ as a case study, the relationship between the modulation index and the minimum inserted SM number is figured in Fig. 7(b). The modulation index is easily changed from 1.0 to 0.5 by increasing the minimum inserted SM number $K$ from 0 to 6. According to (12) and Fig. 7(b), although regulating the parameter $K$ can regulate the voltage gain in a wide range, the regulation is discontinuous because of the integer $K$.

### *D. Modulation Index and Switching Frequency Regulation Based Control Optimization*

Considering the advantages and disadvantages of frequency regulation and modulation index regulation, combining both modulation index regulation and frequency regulation is feasible to extend the input voltage range. The voltage gain from input $U_{\rm in}$ to output $U_{\rm o}$ is expressed as follows:

$$\frac{U_{\rm o}}{U_{\rm in}} = \frac{1}{2} M(N, K) \cdot G(f) \cdot \frac{1}{n} \tag{13}$$

where the first item $M(N, K)$ is the modulation index of MMC, $G(f)$ represents the *LLC* unit gain, $N$ is the MMC arm SM number, and $n$ is the HF transformer turns ratio

$$M(N, K) = \frac{N - K}{N + K}. \tag{14}$$

In (13), these parameters $N$, $n$, $K$, and $f$ have interaction with each other. The hardware parameters design ($N$ and $n$) should consider the control parameters ($K$ and $f$).

The complete block diagram of the proposed modulation index regulation plus switching frequency regulation based voltage control strategy is presented in Fig. 8. First, the modulation index regulation controls the output ac voltage MMC unit according to the input voltage through a feedforward control. The modulation index is changed indirectly by controlling the minimum number of inserted SMs in one period. The function of the modulation index regulation is to obtain an MMC output with a small variation range. Then, the switching frequency is determined by output voltage feedback control, such as a proportional–integral controller. Finally, the SM voltage balancing control scheme is adopted to allocate these drive signals.

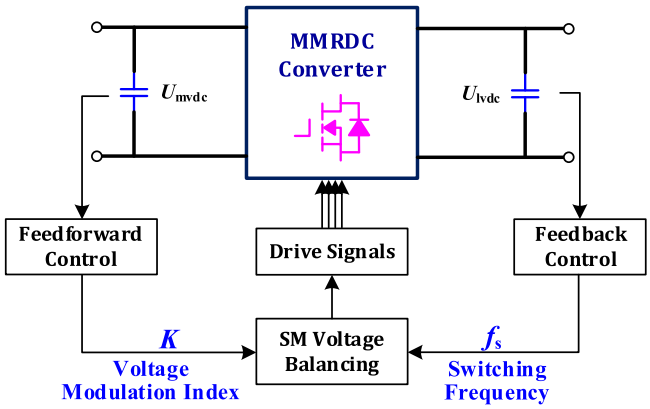


Fig. 8. Wide voltage-gain control block diagram of MMRDC.

TABLE II
KEY PARAMETERS OF TWO CONTROL METHODS

| Parameters | Only frequency regulation | Proposed regulation method |
|---|---|---|
| Input voltage $U_{\rm in}$ | 8 kV~16 kV | |
| Output voltage $U_{\rm o}$ | 375 V | |
| Maximum output power $P_{max}$ | 100 kW | |
| MMC arm SM number $N$ | 20 | 16 |
| Transformer turns ratio $n$ | 18 | 12 |
| $K$ value | 0 | 0, 1, 2, 3, 4, 5 |
| Modulation index | 1 | 1~0.523 |
| Frequency regulation gain $M(f)$ | 0.85~1.7 | 1~1.15 |
| Resonant frequency $f_{\rm r}$ | 12 kHz | 12 kHz |
| Resonant capacitor $C_{\rm r}$ | 215 nF | 300 nF |
| Resonant inductance $L_{\rm r}$ | 800 μH | 600 μH |
| Magnetizing inductance $L_{\rm m}$ | 3mH | 8 mH |
| Switching frequency $f_{\rm sw}$ | 5kHz~25 kHz | 7 kHz ~12 kHz |

In this section, the optimal design and control of MMRDC will be investigated in-depth with a specific example.

For an MVdc to LVdc power supply application, the input voltage range is MV 8–16 kV dc voltage and the output voltage is a constant dc 375 V and the MMRDC maximum output power is 100 kW. If only the frequency regulation is adopted, the key design parameters of the MMRDC converter are listed in the first two columns of Table II. In the study case, supposing that the rated SM voltage is 800 V, there are 20 SMs in each arm to support 16 kV input voltage. To fulfill the frequency regulation gain $G(f)$ requirement, the ratio of resonant inductance $L_{\rm r}$ to magnetizing inductance $L_{\rm m}$ should be relatively large, resulting in a small magnetizing inductance (which is only 3 mH) and a sizeable magnetizing current. The switching frequency range is from 5 to 25 kHz for 8–16 kV input application. Especially under light load working conditions, the switching frequency would be much larger than 25 kHz.

In the proposed control method, to avoid the switching frequency larger than the resonant frequency, the MMRDC always outputs a dc voltage smaller than 375 V when the switching frequency equals the *LLC* resonant frequency. Thus, the switching

TABLE III
SWITCHING POINTS OF $K$ VALUE

| Input voltage | $K$ values | Modulation index |
|---|---|---|
| 8.00 kV ~ 9.07 kV | 0 | 16/16 = 1.00 |
| 9.07 kV ~ 10.29 kV | 1 | 15/17 = 0.88 |
| 10.29 kV ~ 11.69 kV | 2 | 14/18 = 0.78 |
| 11.69 kV ~ 13.33 kV | 3 | 13/19 = 0.68 |
| 13.33 kV ~ 15.27 kV | 4 | 12/20 = 0.60 |
| 15.27 kV ~ 16.00 kV | 5 | 11/21 = 0.52 |

frequency should be set smaller than the resonant frequency to boost the output voltage. When the input voltage is the minimum 8 kV, denoted as $U_{\mathrm{in0}}$, the $K$ value is set to 0. The transformer turns ratio $n$ is designed as 12:1, the LV output dc voltage is 333 V under resonant frequency operation. Then, the *LLC* unit regulates the gain to 1.125 to boost the output voltage to 375 V.

The design principles of the arm SM number $N$ and $K$ value are critical. When the input voltage rises to $U_{\mathrm{in1}}$, which equals $(N+1)/(N-1)\cdot U_{\mathrm{in0}}$, the $K$ value is set to 1. When the input voltage increases to $U_{\mathrm{in2}}$, which equals $(N+2)/(N-2)\cdot U_{\mathrm{in0}}$, the $K$ value is set to 2. In this way, when the input voltage rises to $U_{\mathrm{ink}}$, the $K$ value is set to $k$ ($k = 0,1,2,3,\ldots,$). The $K$ value switching point $U_{\mathrm{ink}}$ ($k=0,1,2,3,\ldots,$) is defined by the following equation:

$$U_{\mathrm{ink}} = \frac{N+k}{N-k}\cdot U_{\mathrm{in0}}, k = 0,1,2,3,\ldots. \tag{15}$$

The MMC arm SM number $N$ and the value $K$ are determined by the input voltage and rated SM voltage $U_{\mathrm{C}}$. Under any $K$ value switching point, the requirement is

$$\frac{U_{\mathrm{ink}}}{N+k} < U_C, k = 0,1,2,3,\ldots. \tag{16}$$

Substituting (15) into (16), we get

$$\frac{U_{\mathrm{in0}}}{N-k} < U_C, k = 0,1,2,3,\ldots. \tag{17}$$

Besides, the maximum $K$ switching point should exceed the maximum input voltage, which is

$$U_{\mathrm{ink,max}} = \frac{N+k_{\max}}{N-k_{\max}}\cdot U_{\mathrm{in0}} > U_{\mathrm{in,max}}. \tag{18}$$

Combining (17) and (18)

$$\begin{cases} \frac{U_{\mathrm{in0}}}{N-k_{\max}} < U_C \\ \frac{N+k_{\max}}{N-k_{\max}} > \frac{U_{\mathrm{in,max}}}{U_{\mathrm{in0}}}. \end{cases} \tag{19}$$

In this study case, $U_{\mathrm{in0}} = 8$ kV, $U_{\mathrm{in,max}} = 16$ kV, $U_{\mathrm{C}} = 800$ V, solve the inequality (19), the minimum arm SM number $N$ is 16, and $k_{\max}$ is 6. The number of arm SMs is reduced by 20% compared with traditional MMC, so the hardware costs and power losses of SMs can be reduced accordingly. The $K$ switching point is listed in Table III. In reality, the switching point $K = 6$ will not be reached.

The following design object is the *LLC* unit. In the proposed regulation method, the *LLC* unit mainly adjusts its gain to stabilize the final output through a feedback control loop. It

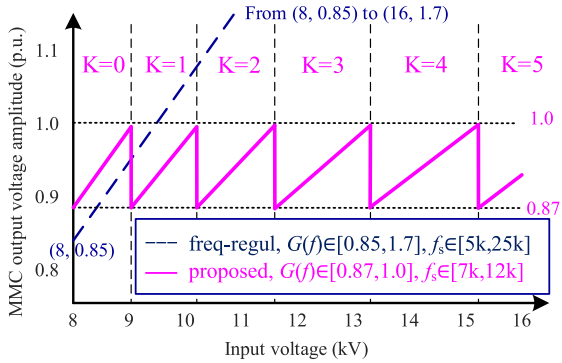


Fig. 9. MMC output voltage amplitude under different input voltages with the proposed regulation method.

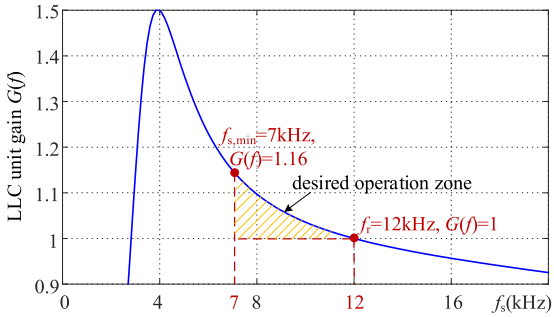


Fig. 10. Desired operation zone of the *LLC* unit in the optimized control.

is easy to prove that when $K$ changes from the maximum $k_{\max}$ to $k_{\max}-1$, the modulation index of MMC has the biggest step change. The change can be calculated according to the following equation:

$$\frac{M(k_{\max}-1)}{M(k_{\max})} = \frac{(N-k_{\max}+1)(N+k_{\max})}{(N+k_{\max}-1)(N-k_{\max})} \tag{20}$$

where $N = 16$, $k_{\max} = 5$, and the maximum change of modulation index is 1.145. So, the *LLC* unit gain range needs to be larger than 1–1.145. The optimal design parameters are shown in the last column of Table II. Compared with the frequency regulation method, the magnetizing inductance (8 mH) is much larger. The switching frequency range is 7–12 kHz, much smaller than that of the frequency regulation method.

With the proposed regulation method, the MMC output voltage amplitude under wide input voltage can be controlled within [0.87, 1.0] (per unit), as demonstrated in Fig. 9. In Fig. 9, the parts where the MMC output voltage amplitude is smaller than 1.0 per unit indicate that the *LLC* unit should decrease the frequency to boost the voltage gain. Therefore, the desired operating range of an *LLC* resonant tank is indicated in Fig. 10. The switching frequency is smaller than the primary resonant voltage $f_{\mathrm{r}}$. Through simulation, Fig. 11 depicts the *LLC* gain curves under different load conditions based on these parameters in Table II. The gain range under light load conditions is a little larger than that under full load conditions. So, the designed *LLC* parameters can fulfill the gain requirement under any load conditions.

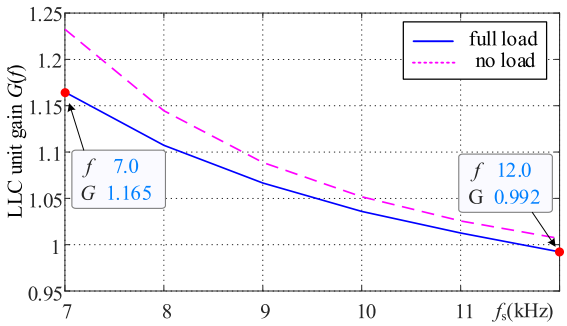


Fig. 11. *LLC* unit gain curves under different load conditions.

## IV. Simulation Results and Experimental Verification

### A. Simulation Results

A simulation model is built in the Plexim/PLECS platform to demonstrate the effectiveness of the proposed design and control strategy. The converter parameters and control optimization design are the same as provided in Tables II and III. The input voltage has a wide range from 8 to 16 kV, the output voltage is controlled to a constant 375 V, and the maximum output power is 100 kW.

The dynamic response of load change is checked through simulation. In Fig. 12, the input voltage stays at 15 kV. When the output power has a step from 1 to 100 kW, the output voltage drop is 15 V. Then, only the feedback loop control changes the switching frequency to boost the *LLC* gain while the modulation index remains unchanged. So, the arm voltage amplitude will not change. The settling time is less than 10 ms. Besides, the SM capacitors get significantly increased ripples with the increased power and decreased switching frequency. When the power drops from 100 to 1 kW, it is the same that only frequency regulation reacts to stabilize the output voltage.

In this study case, the MMC output modulation index has the biggest step jump when the input voltage reaches the point where the $K$ value changes from 4 to 5. So, the simulation waveforms in Fig. 13 illustrate the dynamic behaviors when the changed input voltage causes the modulation index to be regulated accordingly.

As shown in Fig. 13, when the input voltage increases from 15.1 to 15.4 kV, the feedforward control loop regulates the $K$ value from 4 to 5. The MMC arm voltage becomes smaller accordingly when the output voltage rises. So, the feedback control loop needs to decrease the switching frequency to boost the output voltage back to 375 V. To mitigate the overshoot voltage, the switching frequency is adjusted actively as the $K$ value changes. In this way, the output overshoot voltage is smaller than 10 V and the transient response time is less than 3 ms. Moreover, it can be found that the arm voltage is smaller than the input voltage. Hence, the modulation index control can reduce the required SM number or SM capacitor voltages. When the input voltage drops, the control scheme has a similar procedure to stabilize the output voltage.

Fig. 14 illustrates the influence of switching frequency on the voltage stress of arm inductors and the transformer, taking 10 kV/100 kW as an example. From Fig. 14(a), in the nonoptimized

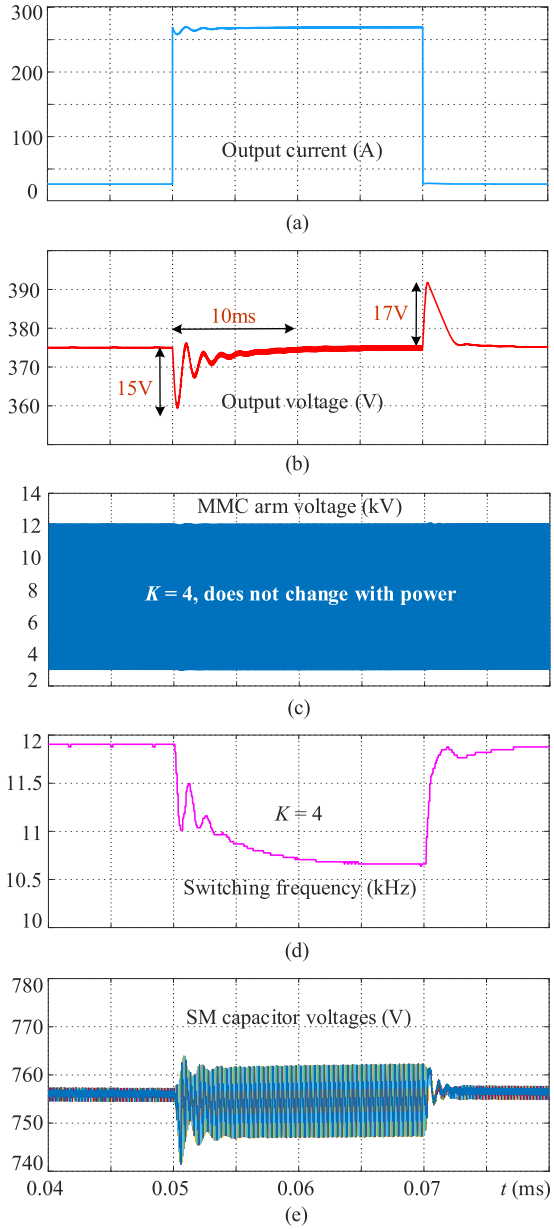


Fig. 12. Dynamic response of the proposed voltage control when output load has step changes. (a) Output current. (b) Output voltage. (c) MMC arm voltage. (d) Switching frequency. (e) SM capacitor voltages.

control scheme, the switching frequency is 20 kHz, which is larger than the primary resonant frequency 12 kHz. The transformer primary voltage is a complete square waveform $\pm 5$ kV with very high $dv/dt$ and the arm inductor voltage stress is about the input voltage level 10 kV. But if the switching frequency is smaller than the resonant frequency 12 kHz, in Fig. 14(b), the secondary side diode current will be discontinuous at the point where arm voltage changes. In this way, the resonant current $i_r$ only contains magnetizing current. The primary input voltage is shared by the MMC arm inductor and the HF transformer at that time. As a result, the arm inductors withstand a resonant voltage of 1.8 kV, much smaller than the input voltage. The primary voltage of the transformer rises gradually with the MMC arm

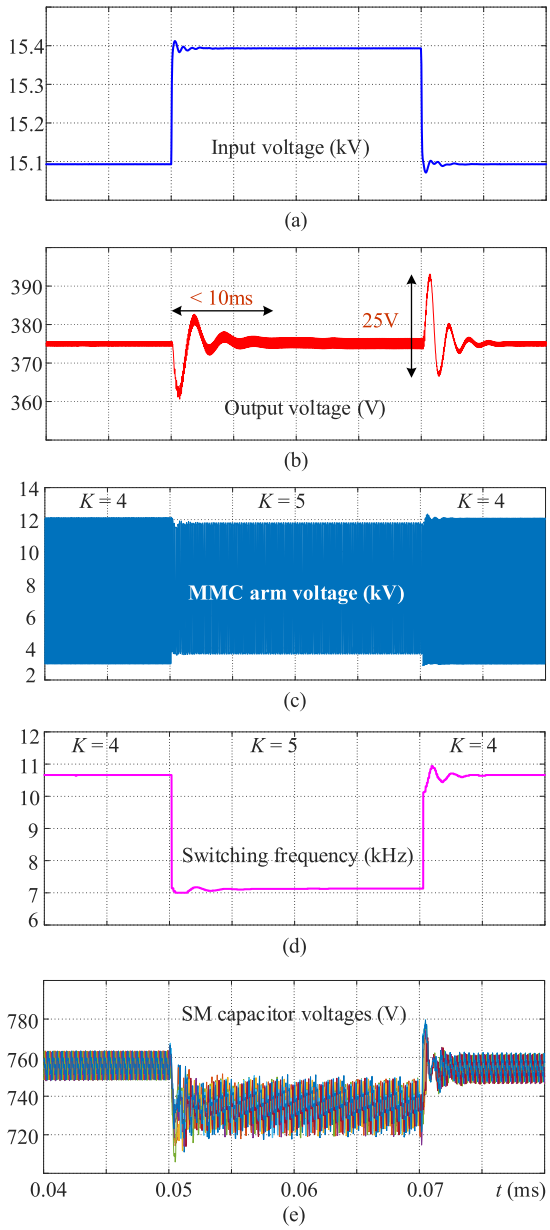


Fig. 13. Dynamic response of the proposed voltage control when input voltage has a step changes. (a) Input voltage. (b) Output voltage. (c) MMC arm voltage. (d) Switching frequency. (e) SM capacitor voltages.

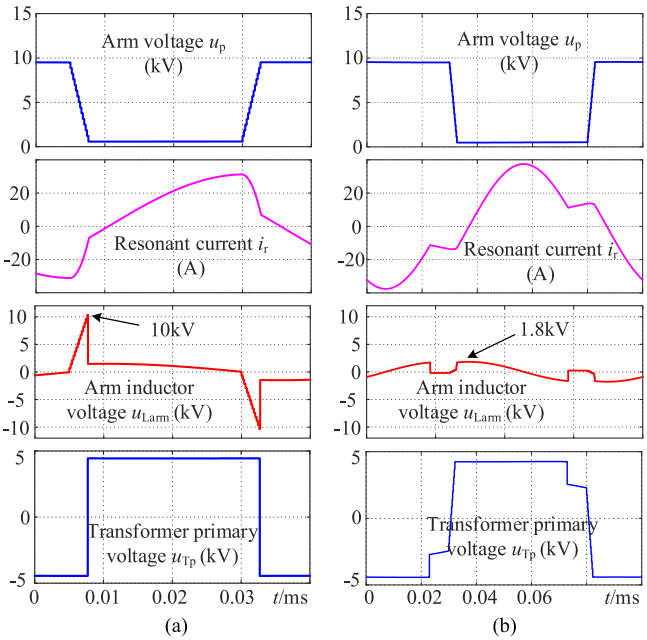


Fig. 14. Waveforms under different switching frequencies. (a) Switching frequency is larger than the resonant frequency in a nonoptimized scheme. (b) Switching frequency is always smaller than the resonant frequency in the proposed optimized scheme.

TABLE IV
KEY PARAMETERS OF THREE CONTROL METHODS

| Parameters | Only frequency regulation | Non-optimized control in [16] | Optimized control in this article |
|---|---|---|---|
| Input voltage $U_{in}$ | 8 kV~16 kV | | |
| Output voltage $U_o$ | 375 V | | |
| Output power $P_{max}$ | 100 kW | | |
| SM switching devices | IKW40N120H3 1200V/40A from Infineon | | |
| Output diode bridge | UFL330FA60 600V/330A from Vishay | | |
| MMC arm SM number $N$ | 20 | 16 | 16 |
| Transformer turns ratio $n$ | 17 | 12 | 12 |
| $K$ value | 0 | 0,1,2,3,4 | 0,1,2,3,4,5 |
| MMC modulation index | 1 | 1~0.60 | 1~0.523 |
| LLC regulation gain $M(f)$ | 0.8~1.6 | 0.94~1.06 | 1~1.15 |
| Resonant frequency $f_r$ | 12 kHz | 12kHz | 12 kHz |
| Resonant capacitor $C_r$ | 215nF | 300 nF | 300 nF |
| Resonant inductance $L_r$ | 800 μH | 700 μH | 600 μH |
| Magnetizing inductance $L_m$ | 3.3mH | 5mH | 8 mH |
| Switching frequency $f_{sw}$ | 5 kHz~ 25 kHz | 6kHz~ 18kHz | 7 kHz ~ 12 kHz |

voltage and the high $dv/dt$ is eliminated. In the optimized control strategy, a switching frequency range smaller than the primary resonant frequency is adopted, so the high voltage stress on the transformer and inductors can be avoided.

The losses of the power devices with three different design and control methods are extracted in the Plexim/PLECS software. These losses under various load conditions and different input voltages are compared in Fig. 15. In these figures, the first control method is the traditional *LLC* frequency regulation, the second is the nonoptimized control method proposed in [16], and the third is the optimized control method proposed in this article. Their design parameters are compared again in Table IV.

According to Fig. 15, the losses of power devices in the frequency regulation method are always the largest, three times higher than those by the other two, especially under low voltage input. This is because the frequency regulation method has the most considerable rms current and the largest number of SMs. The latter two methods have much lower power losses and the losses change little with the wide input range owing to narrower switching frequency. Furthermore, under light load conditions, the optimized control method produces about 25% fewer losses than the nonoptimized method. But with the increment of active power, the power losses difference between

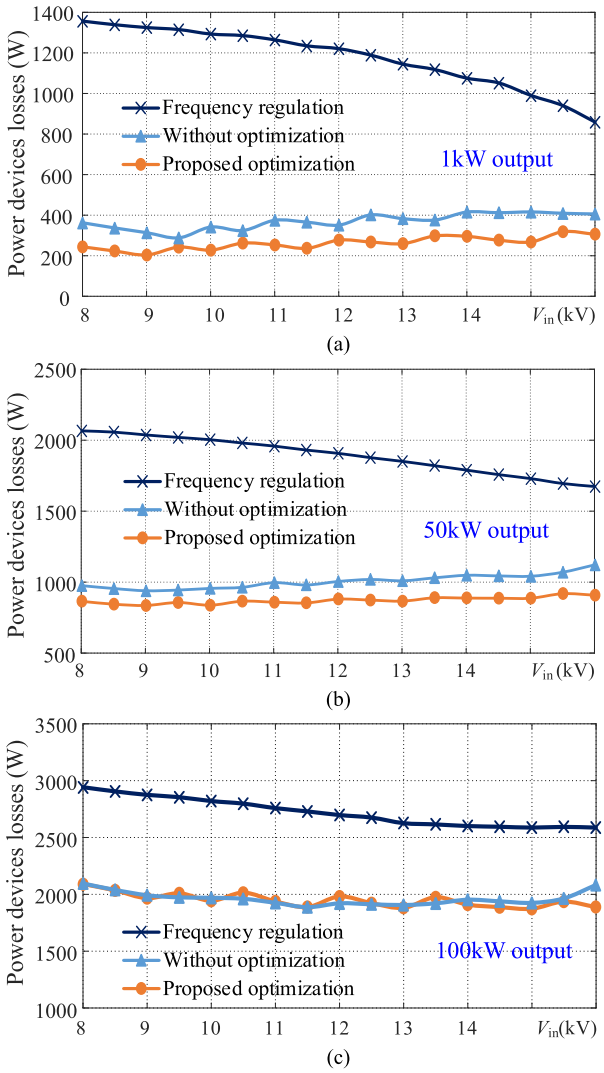


Fig. 15. Losses of switching devices under different input voltages and different load conditions with three different voltage control methods. (a) 1-kW output. (b) 50-kW output. (c) 100-kW output.

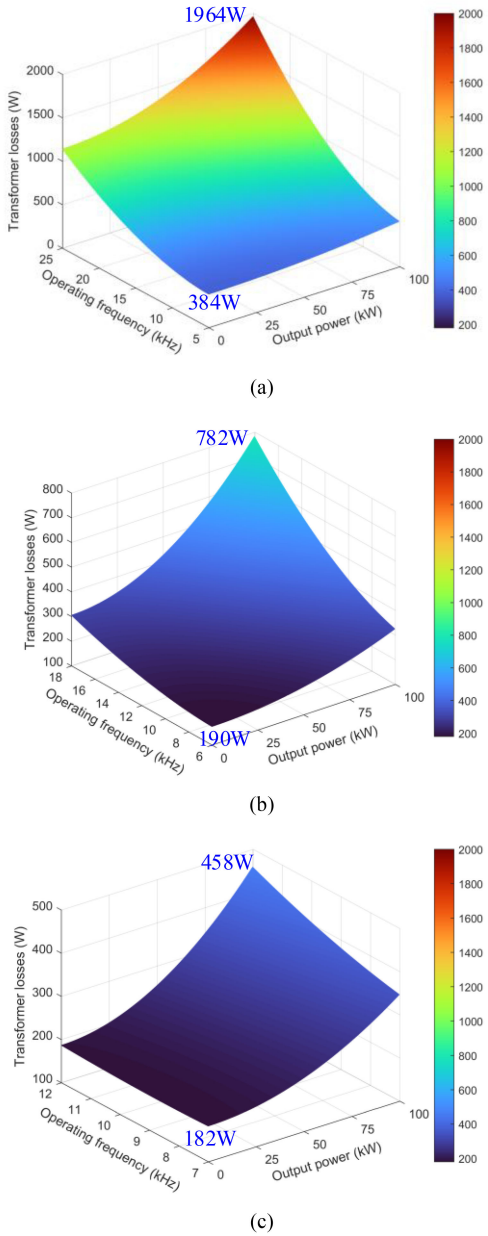


Fig. 16. Losses of HF transformers under different input voltages and different load conditions with three different voltage control methods. (a) With only frequency regulation. (b) With nonoptimized control in [16]. (c) With optimized control in this article.

the two methods is getting smaller. So, the optimized control method has a more significant loss decrease, mainly for light load conditions.

In the MV MMRDC converters, the HF transformer's power losses are crucial and strongly related to its efficiency, power density, and thermal design. Usually, in MVdc applications, the nanocrystalline tapewound cores and litz wires with low losses under high frequency are preferred. The main differences among the transformers in the three control methods are the magnetizing inductance and the operating frequency. First, the magnetizing inductance of the transformer is related to the air gap of the magnetic core. The smaller magnetizing inductance, the larger the air gap of the magnetic core. In this case, a small magnetizing inductance will increase additional copper loss caused by magnetizing current and extra core loss because of the large air gap, especially for nanocrystalline cores [45]. Besides, the transformer with a wider operating frequency range would significantly increase losses.

To be more specific, the improved general Steinmetz formula with the Steinmetz parameters of cores is adopted to calculate the core loss under square wave excitation, and the 1-D Dowell model is used to calculate the ac resistance of the windings [46], [47]. The final results are displayed as a 3-D graph of transformer losses with output power and frequency in Fig. 16. In Fig. 16(a), the minimum losses of the HF transformer with only frequency regulation control are about 384 W, and the losses increase sharply with the operating frequency. When the switching frequency is 25 kHz, the transformer loss is twice more than that of 5 kHz. Maximum losses are incredibly high near 2000 W.

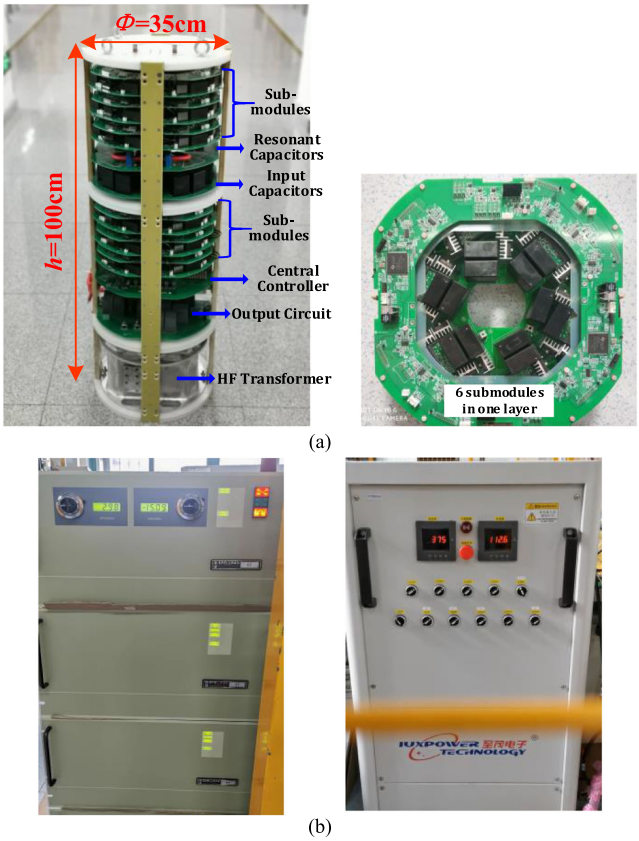


Fig. 17. 16-kV/40-kW laboratory prototype. (a) MMRDC converter structure and its SMs. (b) 16 kV/40 kW medium-voltage dc source and 400 V/40 kW low-voltage dc resistor load.

In Fig. 16(b), with two regulations but nonoptimized control in [16], the power losses of the transformer are reduced by around 50%. Nevertheless, the power losses under maximum operating frequency are still very high, which seriously restricts the improvement of the power density and thermal design of the HF transformer. In this proposed optimized control strategy, the power losses are further decreased from 778 to 458 W. Additionally, with a minor operating frequency from 7 to 12 kHz, the losses vary within 30% under a certain output load. In this method, the high power density and efficiency of the HF transformer under a wide input range can be more easily guaranteed compared with the other two techniques.

### B. Experimental Validation

A 16-kV/60-kW prototype is built in the laboratory to verify the feasibility of the MMRDC topology in MVdc applications and the effectiveness of the proposed voltage control optimization, as shown in Fig. 17(a). The critical design parameters are the same as for the simulation model in Tables II and IV. Other parameters are also listed in Table V. Two redundant SMs are configured for backup in case of SM failure. But limited by the capacity of the medium voltage source and the low voltage load in the lab, this MMRDC converter outputs a maximum power of 40 kW in this experiment. Besides, the arm voltage is not measured due to the lack of high-voltage isolation probes.

TABLE V
EXPERIMENTAL PROTOTYPE PARAMETERS

| Parameters | Value |
|---|---|
| Input voltage | 8kV~16kV |
| Output voltage | 375V |
| Output power | 60kW |
| SM number in one arm | 18 (2 for backups) |
| SM maximum voltage | 800V |
| SM capacitance | 20μF |
| Transformer turns ratio | 12:1 |
| Magnetizing inductance | 8mH |
| Leakage inductance | 600μH |
| Resonant capacitance | 300nF |
| $K$ value | 0,1,2,3,4,5 |
| Modulation index range | [0.565, 1] |
| Switching frequency | 7kHz~12kHz |
| Input capacitor | 2μF |
| Output capacitor | 1mF |

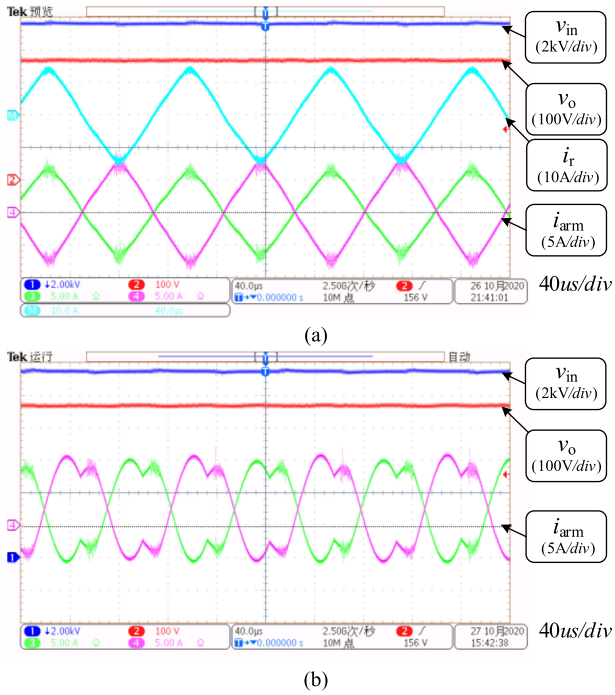


Fig. 18. Arm current under different load conditions. (a) 9.8-kV input and 100-W output. (b) 10.6-kV input and 40-kW output.

In this prototype, three SMs are controlled by one local SM controller to reduce the number of subcontrollers. The auxiliary power of local controllers and power device drivers is self-powered by these distributed SM capacitors, which is easier for medium-voltage isolation. The system status is transmitted to the host computer through Ethernet communication.

Similar to the simulation waveforms shown in Fig. 18(a), the arm current $i_{arm}$ under no-load operation is a triangular waveform with only magnetizing current. The SMs are hard switched in and out at the peak of the arm current, so there will be larger switching loss at light load conditions. The waveforms

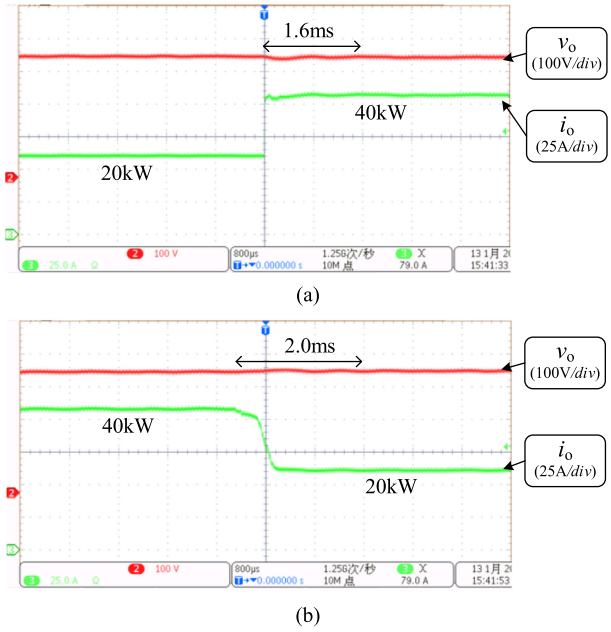


Fig. 19. Load step-change waveforms. (a) 12-kV input, load increases from 20 to 40 kW. (b) 12 kV input, load decreases from 40 to 20 kW.

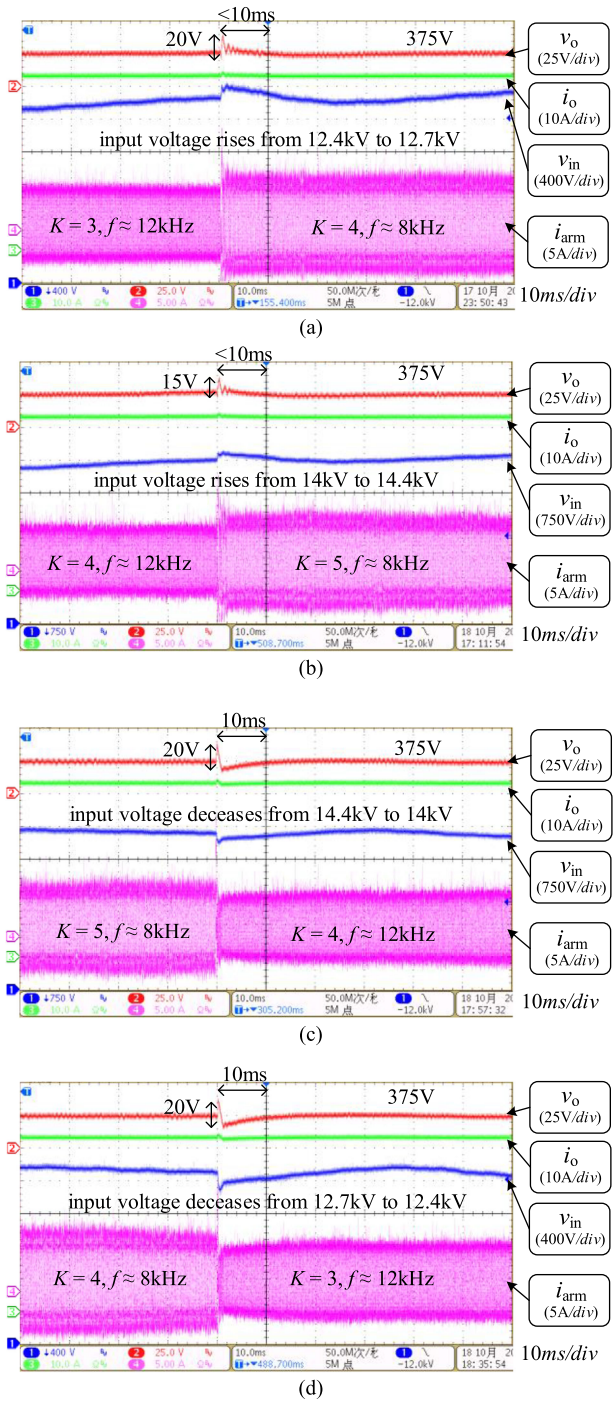


Fig. 20. $K$ value changes with the input voltage. (a) $U_{\text{in}}$ increases from 12.4 to 12.7kV and $K$ changes from 3 to 4. (b) $U_{\text{in}}$ increases from 14.0 to 14.4 kV and $K$ changes from 4 to 5. (c) $U_{\text{in}}$ decreases from 14.4 to 14.0 kV and $K$ changes from 5 to 4. (d) $U_{\text{in}}$ increases from 12.7 to 12.4 kV and $K$ changes from 4 to 3.

under 40-kW output load operation are shown in Fig. 18(b). The arm current consists of three parts, which are dc bias, magnetizing current, and the sinusoidal current. Owing to its dc bias and the magnetizing current, the SMs have opportunities to achieve ZCS under heavy load conditions. Fig. 19 shows the waveforms of load step change under 12 kV input voltage. The output voltage variation is less than 20 V and the transient time is less than 2 ms.

Fig. 20 presents the dynamic behaviors of the proposed voltage control strategy in wide input occasions. The output power is 20 kW in this group of experiments. When the input voltage rises from 12.4 to 12.7 kV, the feedback loop first increases the switching frequency to reduce the *LLC* tank gain. Then, at the $K$ switching point, the feedforward loop changes the modulation index by changing the $K$ value from 3 to 4. The switching frequency is reduced to around 8 kH to boost the voltage gain. Similarly, the $K$ value is adjusted from 4 to 5 if the input voltage increases from 14 to 14.4 kV. During this period, although the dc input voltage is disturbed, the output voltage overshoot is only 20 V and it takes 10 ms to get back to a steady state. Because the magnetizing current is inversely proportional to the switching frequency, the arm current amplitudes under 8 and 12 kHz are different. When the input voltage decreases across $K$ switching points, the waveforms of $K$ value decreasing have a similar process. Furthermore, a hysteresis control is set in the actual implementation to prevent the feedforward control loop from oscillating.

The converter's power losses and conversion efficiency are measured in this experiment. Under the working condition of 12-kV input and 40-kW output, the losses composition is presented in Fig. 21. The MMC SMs contribute more than half of the total losses, and the switching losses are even less than the conduction losses owing to its soft-switching operation. The LV-side diodes have about a quarter of losses. The transformer, auxiliary power supply, and other components produce about 20% losses.

The efficiency and power losses with different output power are plotted in Figs. 22 and 23. From Fig. 22, the system efficiency increases with the output power. The efficiency exceeds 92% at 10-kW output and can reach 96% above 30-kW output. The

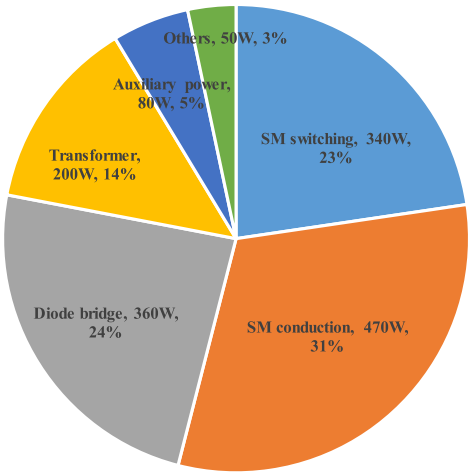


Fig. 21. Losses composition of the laboratory MMRDC prototype under 12 kV/40 kW working condition.

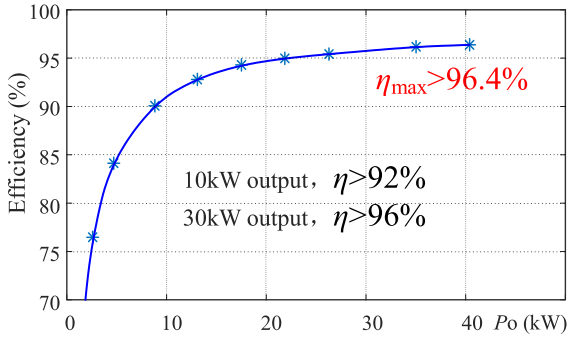


Fig. 22. System efficiency under different output powers.

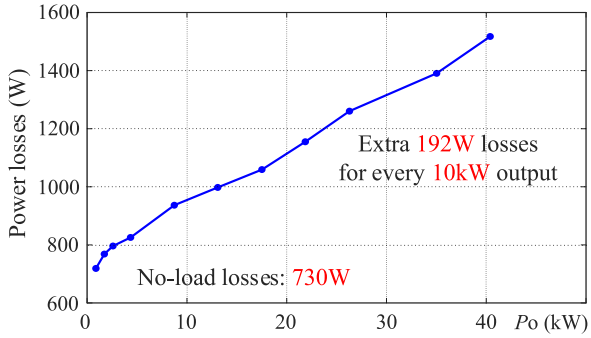


Fig. 23. Relationship between power losses and output power.

efficiency is relatively low under light load considering the magnetizing current in the arm current. According to Fig. 23, the power loss under no-load conditions is about 730 W, so the efficiency under light load conditions is not high. Nevertheless, only about 192-W losses are produced for every 10-kW output. Hence, it can be predicted that the efficiency can reach 97% under 60-kW output. Furthermore, the efficiency under different input voltages is tested, as illustrated in Fig. 24. Ignoring the measurement error, the efficiency under different input voltage remains the same, over 92% with 10-kW output, over 95% with 20-kW output, and over 96% with 40-kW output. These results

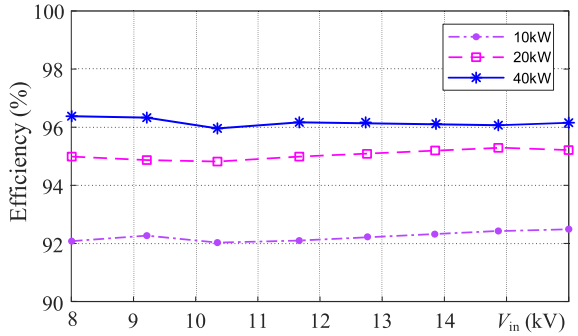


Fig. 24. System efficiency under different input voltages.

demonstrate the high efficiency under a wide input range by employing the proposed voltage control strategy.

## V. Conclusion

In this article, the modulation index regulation and frequency regulation based control optimization is proposed to adjust the output voltage of modular MMRDC for wide-input-voltage-range applications. The optimal control parameters design is investigated detailedly. Compared with only frequency regulation of an *LLC* unit, the MMC SM number can be reduced by 20%, the transformer magnetizing current is reduced to about 40%, and the switching frequency regulation range is reduced to 25%. All these improvements can bring a loss reduction for power devices and the HF transformer, particularly. Furthermore, the optimally designed switching frequency is always smaller than the *LLC* resonant frequency, which brings a narrower frequency regulation range under light load conditions. The optimized control can avoid undesired high-voltage stress on arm inductors and high *dv*/*dt* on the transformer. Based on the optimized voltage control strategy, an 8–16 kV input, 375 V/60 kW output MMRDC prototype has been developed in the laboratory and the experimental results verified the effectiveness of the voltage regulation strategy. Under such a wide-range input voltage, the system efficiency can keep over 96% under 40-kW load conditions.

## References

[1] S. Kenzelmann, A. Rufer, D. Dujic, F. Canales, and Y. R. de Novaes, "Isolated DC/DC structure based on modular multilevel converter," *IEEE Trans. Power Electron.*, vol. 30, no. 1, pp. 89–98, Jan. 2015.

[2] L. Shu *et al.*, "A resonant ZVZCS DC-DC converter with two uneven transformers for an MVdc collection system of offshore wind farms," *IEEE Trans. Ind. Electron.*, vol. 64, no. 10, pp. 7886–7895, Oct. 2017.

[3] S. Du, B. Wu, N. R. Zargari, and Z. Cheng, "A flying-capacitor modular multilevel converter for medium-voltage motor drive," *IEEE Trans. Power Electron.*, vol. 32, no. 3, pp. 2081–2089, Mar. 2017.

[4] D. Rothmund, T. Guillod, D. Bortis, and J. W. Kolar, "99% efficient 10 kV SiC-based 7 kV/400 V DC transformer for future data centers," *IEEE J. Emerg. Sel. Topics Power Electron.*, vol. 7, no. 2, pp. 753–767, Jun. 2019.

[5] S. Inoue and H. Akagi, "A bidirectional isolated DC–DC converter as a core circuit of the next-generation medium-voltage power conversion system," *IEEE Trans. Power Electron.*, vol. 22, no. 2, pp. 535–542, Mar. 2007.

[6] W. Chen, A. Q. Huang, C. Li, G. Wang, and W. Gu, "Analysis and comparison of medium voltage high power DC/DC converters for offshore wind energy systems," *IEEE Trans. Power Electron.*, vol. 28, no. 4, pp. 2014–2023, Apr. 2013.

[7] F. Deng and Z. Chen, "Control of improved full-bridge three-level DC/DC converter for wind turbines in a DC grid," *IEEE Trans. Power Electron.*, vol. 28, no. 1, pp. 314–324, Jan. 2013.

[8] W. Li and X. He, "Review of nonisolated high-step-up DC/DC converters in photovoltaic grid-connected applications," *IEEE Trans. Ind. Electron.*, vol. 58, no. 4, pp. 1239–1250, Apr. 2011.

[9] Z. Lu *et al.*, "Medium voltage soft-switching DC/DC converter with series-connected SiC MOSFETs," *IEEE Trans. Power Electron.*, vol. 36, no. 2, pp. 1451–1462, Feb. 2021.

[10] D. Ma, W. Chen, and X. Ruan, "A review of voltage/current sharing techniques for series–parallel-connected modular power conversion systems," *IEEE Trans. Power Electron.*, vol. 35, no. 11, pp. 12383–12400, Nov. 2020.

[11] L. Wang, Q. Zhu, W. Yu, and A. Q. Huang, "A medium-voltage medium-frequency isolated DC–DC converter based on 15-kV SiC MOSFETs," *IEEE J. Emerg. Sel. Topics Power Electron.*, vol. 5, no. 1, pp. 100–109, Mar. 2017.

[12] B. Zhao, Q. Song, J. Li, Q. Sun, and W. Liu, "Full-process operation, control, and experiments of modular high-frequency-link DC transformer based on dual active bridge for flexible MVdc distribution: A practical tutorial," *IEEE Trans. Power Electron.*, vol. 32, no. 9, pp. 6751–6766, Sep. 2017.

[13] B. Zhao, Q. Song, J. Li, X. Xu, and W. Liu, "Comparative analysis of multilevel-high-frequency-link and multilevel-DC-link DC-DC transformers based on MMC and dual-active bridge for MVdc application," *IEEE Trans. Power Electron.*, vol. 33, no. 3, pp. 2035–2049, Mar. 2018.

[14] H. Liu, M. S. A. Dahidah, J. Yu, R. T. Naayagi, and M. Armstrong, "Design and control of unidirectional DC-DC modular multilevel converter for offshore DC collection point: Theoretical analysis and experimental validation," *IEEE Trans. Power Electron.*, vol. 34, no. 6, pp. 5191–5208, Jun. 2019.

[15] X. Zhang and T. C. Green, "The modular multilevel converter for high step-up ratio DC-DC conversion," *IEEE Trans. Ind. Electron.*, vol. 62, no. 8, pp. 4925–4936, Aug. 2015.

[16] S. Shao *et al.*, "A modular multilevel resonant DC-DC converter," *IEEE Trans. Power Electron.*, vol. 35, no. 8, pp. 7921–7932, Aug. 2020.

[17] Z. Lu, L. Lin, X. Wang, and C. Xu, "LLC-MMC resonant DC-DC converter: Modulation method and capacitor voltage balance control strategy," in *Proc. IEEE Appl. Power Electron. Conf. Expo.*, 2020, pp. 2056–2061.

[18] X. Xiang, X. Zhang, T. Luth, M. M. C. Merlin, and T. C. Green, "A compact modular multilevel DC-DC converter for high step-ratio MV and HV use," *IEEE Trans. Ind. Electron.*, vol. 65, no. 9, pp. 7060–7071, Sep. 2018.

[19] X. Xiang, X. Zhang, G. P. Chaffey, and T. C. Green, "An isolated resonant mode modular converter with flexible modulation and variety of configurations for MVdc application," *IEEE Trans. Power Del.*, vol. 33, no. 1, pp. 508–519, Feb. 2018.

[20] Z. Xing, X. Ruan, H. You, X. Yang, D. Yao, and C. Yuan, "Soft-switching operation of isolated modular DC/DC converters for application in HVDC grids," *IEEE Trans. Power Electron.*, vol. 31, no. 4, pp. 2753–2766, Apr. 2016.

[21] T. Luth, M. M. C. Merlin, T. C. Green, F. Hassan, and C. D. Barker, "High-frequency operation of a DC/AC/DC system for HVDC applications," *IEEE Trans. Power Electron.*, vol. 29, no. 8, pp. 4107–4115, Aug. 2014.

[22] M. I. A. R. Stephan Kenzelmann and M. I. A. O. Francisco Canales, "Isolated DC-DC structure based on modular multilevel converters," *IEEE Trans. Power Electron.*, vol. 30, no. 1, pp. 89–98, Jan. 2015.

[23] Y. Shi and H. Li, "Isolated modular multilevel DC-DC converter with DC fault current control capability based on current-fed dual active bridge for MVdc application," *IEEE Trans. Power Electron.*, vol. 33, no. 3, pp. 2145–2161, Mar. 2018.

[24] B. Zhao, Q. Song, J. Li, Y. Wang, and W. Liu, "High-frequency-link modulation methodology of DC-DC transformer based on modular multilevel converter for HVDC application: Comprehensive analysis and experimental verification," *IEEE Trans. Power Electron.*, vol. 32, no. 5, pp. 3413–3424, May 2017.

[25] C. Sun, J. Zhang, Y. Chang, G. Shi, and X. Cai, "Wide voltage range operation of isolated modular multilevel DC-DC converter," in *Proc. 41st Annu. Conf. IEEE Ind. Electron. Soc.*, 2015, pp. 4953–4958.

[26] M. Narimani, B. Wu, Z. Cheng, and N. R. Zargari, "A new nested neutral point-clamped (NNPC) converter for medium-voltage (MV) power conversion," *IEEE Trans. Power Electron.*, vol. 29, no. 12, pp. 6375–6382, Dec. 2014.

[27] W. Ye, W. Cui, S. Shao, J. Zhang, and K. Sheng, "A resonant DC-DC converter with modular rectifier for high voltage gain and wide output voltage range applications," in *Proc. 45th Annu. Conf. IEEE Ind. Electron. Soc.*, 2019, pp. 6671–6676.

[28] H. Moradisizkoohi, N. Elsayad, and O. A. Mohammed, "A bipolar DC-DC converter with wide voltage-gain range for energy storage integration in ship power systems," in *Proc. IEEE Electr. Ship Technol. Symp.*, 2019, pp. 511–517.

[29] M. A. El-Sharkawi *et al.*, "North east pacific time-integrated undersea networked experiments (NEPTUNE): Cable switching and protection, " *IEEE J. Ocean. Eng.*, vol. 30, no. 1, pp. 232–240, Jun. 2005.

[30] N. R. Butler *et al.*, "Undersea MVdc power distribution," in *Proc. IEEE Int. Power Modulator High Voltage Conf.*, 2010, pp. 294–297.

[31] F. Lu, H. Zhou, J. Yue, X. Peng, B. He, and Z. Wu, "Design of an undersea power system for the east China sea experimental cabled seafloor observatory," in *Proc. OCEANS - San Diego*, 2013, pp. 1–6.

[32] I. A. Gowaid, G. P. Adam, A. M. Massoud, S. Ahmed, D. Holliday, and B. W. Williams, "Quasi two-level operation of modular multilevel converter for use in a high-power DC transformer with DC fault isolation capability," *IEEE Trans. Power Electron.*, vol. 30, no. 1, pp. 108–123, Jan. 2015.

[33] I. A. Gowaid, G. P. Adam, S. Ahmed, D. Holliday, and B. W. Williams, "Analysis and design of a modular multilevel converter with trapezoidal modulation for medium and high voltage DC-DC transformers," *IEEE Trans. Power Electron.*, vol. 30, no. 10, pp. 5439–5457, Oct. 2015.

[34] B. Zhao, Q. Song, J. Li, Y. Wang, and W. Liu, "High-frequency-link modulation methodology of DC–DC transformer based on modular multilevel converter for HVDC application: Comprehensive analysis and experimental verification," *IEEE Trans. Power Electron.*, vol. 32, no. 5, pp. 3413–3424, May 2017.

[35] B. Zhao, Q. Song, J. Li, Y. Wang, and W. Liu, "Modular multilevel high-frequency-link DC transformer based on dual active phase-shift principle for medium-voltage DC power distribution application," *IEEE Trans. Power Electron.*, vol. 32, no. 3, pp. 1779–1791, Mar. 2017.

[36] Y. Wang, Q. Song, B. Zhao, J. Li, Q. Sun, and W. Liu, "Quasi-square-wave modulation of modular multilevel high-frequency DC converter for medium-voltage DC distribution application," *IEEE Trans. Power Electron.*, vol. 33, no. 9, pp. 7480–7495, Sep. 2018.

[37] H. Bai and C. Mi, "Eliminate reactive power and increase system efficiency of isolated bidirectional dual-active-bridge DC-DC converters using novel dual-phase-shift control," *IEEE Trans. Power Electron.*, vol. 23, no. 6, pp. 2905–2914, Nov. 2008.

[38] J. Narli, H. D. Tafti, G. G. Farivar, J. Pou, B. X. Nguyen, and K. L. Hai, "Control scheme for LLC resonant converter with improved performance under light loads and wide input-output voltage variation," in *Proc. IEEE Energy Convers. Congr. Expo.*, 2019, pp. 1605–1608.

[39] C. Yeon, J. Kim, M. Park, I. Lee, and G. Moon, "Improving the light-load regulation capability of LLC series resonant converter using impedance analysis," *IEEE Trans. Power Electron.*, vol. 32, no. 9, pp. 7056–7067, Sep. 2017.

[40] Y. Chen, S. Zhao, Z. Li, X. Wei, and Y. Kang, "Modeling and control of the isolated DC-DC modular multilevel converter for electric ship medium voltage direct current power system," *IEEE J. Emerg. Sel. Topics Power Electron.*, vol. 5, no. 1, pp. 124–139, Mar. 2017.

[41] X. Wei, Y. Chen, X. Wang, Y. Kang, and Y. Cui, "Design and implementation of the low computational burden phase-shifted modulation for DC-DC modular multilevel converter," *IET Power Electron.*, vol. 9, no. 2, pp. 256–269, 2016.

[42] S. Shao, M. Jiang, J. Zhang, and X. Wu, "A capacitor voltage balancing method for a modular multilevel DC transformer for DC distribution system," *IEEE Trans. Power Electron.*, vol. 33, no. 4, pp. 3002–3011, Apr. 2018.

[43] J. Liu, J. Zhang, T. Q. Zheng, and J. Yang, "A modified gain model and the corresponding design method for an LLC resonant converter," *IEEE Trans. Power Electron.*, vol. 32, no. 9, pp. 6716–6727, Sep. 2017.

[44] X. Xiang *et al.*, "Resonant modular multilevel DC–DC converters for both high and low step-ratio connections in MVdc distribution systems," *IEEE Trans. Power Electron.*, vol. 36, no. 7, pp. 7625–7640, Jul. 2021.

[45] G. Calderon-Lopez, Y. Wang, and A. J. Forsyth, "Mitigation of gap losses in nanocrystalline tape-wound cores," *IEEE Trans. Power Electron.*, vol. 34, no. 5, pp. 4656–4664, May 2019.

[46] M. Mogorovic and D. Dujic, "100 kW, 10 kHz medium-frequency transformer design optimization and experimental verification," *IEEE Trans. Power Electron.*, vol. 34, no. 2, pp. 1696–1708, Feb. 2019.

[47] R. Lu, J. Sheng, Y. Yao, C. Li, W. Li, and X. He, "Design and verification of a high ratio medium frequency transformer for subsea power conversion," in *Proc. IEEE 12th Energy Convers. Congr. Expo. - Asia*, 2021, pp. 886–892.

**Jing Sheng** (Graduate Student Member, IEEE) was born in Anhui, China, in 1993. He received the B.S. degree in 2017 from the College of Electrical Engineering, Zhejiang University, Hangzhou, China, where he is currently working toward the Ph.D. degree in electrical engineering.

His current research interests include modulation and control of medium-voltage modular multilevel converters.

**Cong Chen** received the B.Sc. degree in electrical engineering and its automation from the Harbin Institute of Technology, Harbin, China, in 2020. He is currently working toward the M.Sc. degree in electrical engineering from Zhejiang University, Hangzhou, China.

His research interests include the modulation and control of modular multilevel converters.

**Rui Lu** (Graduate Student Member, IEEE) was born in Liaoning, China. He received the B.S. degree in electrical engineering in 2018 from the College of Electrical Engineering, Zhejiang University, Hangzhou, China. He is currently working toward the Ph.D. degree in electrical engineering with Zhejiang University–University of Illinois at Urbana-Champaign Institute, Zhejiang, China.

His research interests include modeling and design of medium-voltage high-frequency magnetic components and high power converters.

**Chushan Li** (Member, IEEE) received the B.E.E. and Ph.D. degrees in electrical engineering from the Department of Electrical Engineering, Zhejiang University, Hangzhou, China, in 2008 and 2014, respectively.

He is currently an Assistant Professor with Zhejiang University–University of Illinois at Urbana-Champaign Institute, Zhejiang, China. From April 2008 to September 2008, he was an internship student with the Power Application Design Center in National Semiconductor Hong Kong Co., Ltd., Hong Kong. From December 2010 to October 2011, he was a visiting scholar with FREEDM Center, North Carolina State University, Raleigh, NC, USA. From December 2013 to June 2014, he was a research assistant with Hong Kong Polytechnic University, Hong Kong. From July 2014 to July 2017, he was a Postdoctoral Fellow with the Department of Electrical and Computer Engineering, Ryerson University, Toronto, ON, Canada. His research interests include high-power density power converter design and AC–DC power conversion.

**Xin Xiang** (Member, IEEE) received the B.Sc. degree from the Harbin Institute of Technology, Harbin, China, in 2011, the M.Sc. degree from Zhejiang University, Hangzhou, China, in 2014, and the Ph.D. degree from the Imperial College London, London, U.K., in 2018, all in electrical and electronic engineering.

From 2018 to 2020, he was a Research Associate with Imperial College London. He is currently a tenure-track Associate Professor with the College of Electrical Engineering, Zhejiang University, Hangzhou, China. His research interests include the analysis and control of power electronics converters for power system applications.

Dr. Xiang was the recipient of the Eryl Cadwaladr Davies Prize for the Best Ph.D. Thesis of Electrical and Electronic Engineering Department, Imperial College London and the Best Ph.D. Thesis Award from IEEE PELS U.K. and Ireland Chapter.

**Wuhua Li** (Member, IEEE) received the B.Sc. and Ph.D. degrees in power electronics and electrical engineering from Zhejiang University, Hangzhou, China, in 2002 and 2008, respectively.

From 2004 to 2005, he was a Research Intern, and from 2007 to 2008, a Research Assistant with GE Global Research Center, Shanghai, China. From 2008 to 2010, he joined the College of Electrical Engineering, Zhejiang University, as a Postdoctoral Researcher. In 2010, he was promoted to Associate Professor. Since 2013, he has been a Full Professor with Zhejiang University. From 2010 to 2011, he was a Ryerson University Postdoctoral Fellow with the Department of Electrical and Computer Engineering, Ryerson University, Toronto, ON, Canada. He is currently the Executive Deputy Director of the National Specialty Laboratory for Power Electronics and the Vice Director of Power Electronics Research Institute, Zhejiang University. His research interests include power devices, converter topologies, and advanced controls for high power energy conversion systems. He has authored or coauthored more than 300 peer-reviewed technical papers and holds more than 50 issued/pending patents.

Dr. Li is currently an Associate Editor for the *Journal of Emerging and Selected Topics in Power Electronics*, *IET Power Electronics*, *CSEE Journal of Power and Energy Systems*, *CPSS Transactions on Power Electronics and Applications*, *Proceedings of the Chinese Society for Electrical Engineering*, a Guest Editor for *IET Renewable Power Generation* for Special Issue "DC and HVDC system technologies," and Member of Editorial Board for the *Journal of Modern Power System and Clean Energy*. He, due to his excellent teaching and research contributions, was the recipient of the 2012 Delta Young Scholar from Delta Environmental and Educational Foundation, 2012 Outstanding Young Scholar from National Science Foundation of China, 2013 Chief Youth Scientist of National 973 Program, 2014 Young Top-Notch Scholar of National Ten Thousand Talent Program, and 2019 Distinguished Young Scholar from National Science Foundation of China. He was also the recipient of one National Natural Science Award and four Scientific and Technological Achievement Awards from Zhejiang Provincial Government and the State Educational Ministry of China. Since 2014, he has been appointed as the Most Cited Chinese Researchers by Elsevier.

**Xiangning He** (Fellow, IEEE) received the B.Sc. and M.Sc. degrees from the Nanjing University of Aeronautical and Astronautical, Nanjing, China, in 1982 and 1985, respectively, and the Ph.D. degree from Zhejiang University, Hangzhou, China, in 1989.

From 1985 to 1986, he was an Assistant Engineer with the 608 Institute of Aeronautical Industrial General Company, Zhuzhou, China. From 1989 to 1991, he was a Lecturer with Zhejiang University. In 1991, he obtained a Fellowship from the Royal Society of U.K., and conducted research in the Department of Computing and Electrical Engineering, Heriot-Watt University, Edinburgh, U.K., as a Postdoctoral Research Fellow for two years. In 1994, he joined Zhejiang University as an Associate Professor. Since 1996, he has been a Full Professor with the College of Electrical Engineering, Zhejiang University. He was the Director of the Power Electronics Research Institute, the Head of the Department of Applied Electronics, and the Vice Dean of the College of Electrical Engineering. He is currently the Director of the National Specialty Laboratory for Power Electronics, Zhejiang University. His research interests include power electronics and their industrial applications.

Dr. He was appointed as the IEEE Distinguished Lecturer by the IEEE Power Electronics Society (2011–2015). He is also a Fellow of the Institution of Engineering and Technology (formerly IEE), U.K.